



## Article

# Ground-Based MAX-DOAS Observations of Tropospheric NO<sub>2</sub> and HCHO During COVID-19 Lockdown and Spring Festival Over Shanghai, China

Aimon Tanvir<sup>1</sup>, Zeeshan Javed<sup>2</sup> , Zhu Jian<sup>1</sup>, Sanbao Zhang<sup>1</sup>, Muhammad Bilal<sup>3</sup> , Ruibin Xue<sup>1</sup>, Shanshan Wang<sup>1,4,5</sup> and Zhou Bin<sup>1,4,5,\*</sup>

- <sup>1</sup> Shanghai Key Laboratory of Atmospheric Particle Pollution and Prevention (LAP3), Department of Environmental Science and Engineering, Fudan University, Shanghai 200433, China; 19110740045@fudan.edu.cn (A.T.); 20110740023@fudan.edu.cn (Z.J.); 18210740015@fudan.edu.cn (S.Z.); 18210740013@fudan.edu.cn (R.X.)
- <sup>2</sup> Collaborative Innovation Center of Atmospheric Environment and Equipment Technology, Jiangsu Key Laboratory of Atmospheric Environment Monitoring and Pollution Control, School of Environmental Science and Engineering, Nanjing University of Information Science and Technology, Nanjing 210044, China; zeeshan@mail.ustc.edu.cn
- <sup>3</sup> School of Marine Sciences, Nanjing University of Information Science and Technology, Nanjing 210044, China; muhammad.bilal@connect.polyu.hk
- <sup>4</sup> Institute of Atmospheric Sciences, Fudan University, Shanghai 200433, China; shanshanwang@fudan.edu.cn
- <sup>5</sup> Shanghai Institute of Eco-Chongming (SIEC), No.3663 Northern Zhongshan Road, Shanghai 200062, China
- \* Correspondence: binzhou@fudan.edu.cn



**Citation:** Tanvir, A.; Javed, Z.; Jian, Z.; Zhang, S.; Bilal, M.; Xue, R.; Wang, S.; Bin, Z. Ground-Based MAX-DOAS Observations of Tropospheric NO<sub>2</sub> and HCHO During COVID-19 Lockdown and Spring Festival Over Shanghai, China. *Remote Sens.* **2021**, *13*, 488. <https://doi.org/10.3390/rs13030488>

Academic Editor: Maria João Costa  
Received: 6 January 2021  
Accepted: 28 January 2021  
Published: 30 January 2021

**Publisher's Note:** MDPI stays neutral with regard to jurisdictional claims in published maps and institutional affiliations.



**Copyright:** © 2021 by the authors. Licensee MDPI, Basel, Switzerland. This article is an open access article distributed under the terms and conditions of the Creative Commons Attribution (CC BY) license (<https://creativecommons.org/licenses/by/4.0/>).

**Abstract:** Reduced mobility and less anthropogenic activity under special case circumstances over various parts of the world have pronounced effects on air quality. The objective of this study is to investigate the impact of reduced anthropogenic activity on air quality in the mega city of Shanghai, China. Observations from the highly sophisticated multi-axis differential optical absorption spectroscope (MAX-DOAS) instrument were used for nitrogen dioxide (NO<sub>2</sub>) and formaldehyde (HCHO) column densities. In situ measurements for NO<sub>2</sub>, ozone (O<sub>3</sub>), particulate matter (PM<sub>2.5</sub>) and the air quality index (AQI) were also used. The concentration of trace gases in the atmosphere reduces significantly during annual Spring Festival holidays, whereby mobility is reduced and anthropogenic activities come to a halt. The COVID-19 lockdown during 2020 resulted in a considerable drop in vertical column densities (VCDs) of HCHO and NO<sub>2</sub> during lockdown Level-1, which refers to strict lockdown, i.e., strict measures taken to reduce mobility (43% for NO<sub>2</sub>; 24% for HCHO), and lockdown Level-2, which refers to relaxed lockdown, i.e., when the mobility restrictions were relaxed somehow (20% for NO<sub>2</sub>; 22% for HCHO), compared with pre-lockdown days, as measured by the MAX-DOAS instrument. However, for 2019, a reduction in VCDs was found only during Level-1 (24% for NO<sub>2</sub>; 6.62% for HCHO), when the Spring Festival happened. The weekly cycle for NO<sub>2</sub> and HCHO depicts no significant effect of weekends on the lockdown. After the start of the Spring Festival, the VCDs of NO<sub>2</sub> and HCHO showed a decline for 2019 as well as 2020. Backward trajectories calculated using the Hybrid Single-Particle Lagrangian Integrated Trajectory (HYSPLIT) model indicated more air masses coming from the sea after the Spring Festival for 2019 and 2020, implying that a low pollutant load was carried by them. No impact of anthropogenic activity was found on O<sub>3</sub> concentration. The results indicate that the ratio of HCHO to NO<sub>2</sub> (RFN) fell in the volatile organic compound (VOC)-limited regime.

**Keywords:** NO<sub>2</sub>; HCHO; MAX-DOAS; remote sensing; Spring Festival

## 1. Introduction

Nitrogen dioxide (NO<sub>2</sub>) and formaldehyde (HCHO) are two important trace gas species in the atmosphere which play a key role in defining the atmospheric chemistry.

Their concentration may vary depending on certain physical conditions and chemical or photochemical processes. Meteorology is an important factor which plays a significant role in determining the chemical composition of the atmosphere as it largely impacts the residence time of trace gas species [1,2]. NO<sub>2</sub> has detrimental impacts on air quality as it holds a key role in defining tropospheric chemistry [3]. As a precursor for secondary organic aerosols and a component of catalytic cycles that lead to the formation of tropospheric ozone (O<sub>3</sub>), this gas is a crucial atmospheric pollutant [4,5]. Nitric acid is the oxidation product of NO<sub>2</sub> which can be deposited either in dry or precipitate form [6]. Biomass burning, fossil fuel combustion, soil emissions and natural lightening are some of the sources of NO<sub>2</sub> in the atmosphere [7]. For most urban settlements, NO<sub>x</sub> comes predominantly from anthropogenic sources including vehicle exhausts, industrial processes and power generation. As NO<sub>x</sub> has a residence time of the order of a few hours in the lower troposphere, it is usually found close to sources under calm meteorological conditions [8]. Formaldehyde (HCHO) is a short-lived atmospheric species which comes from the oxidation of volatile organic compounds (VOCs) in the atmosphere. The tropospheric variability of HCHO largely depends on the oxidation of non-methane VOCs (NMVOCs) of pyrogenic, biogenic and anthropogenic origins [1]. Direct emissions may result from fossil fuel and biomass burning as well as from natural vegetation. HCHO is employed as a tracer of VOCs owing to its short life span [9]. Both HCHO and NO<sub>2</sub> play a significant role in defining atmospheric composition and their ratio (RFN) is used as a proxy for tropospheric O<sub>3</sub> production [10,11].

Human footprints on the environment result in an upsurge in the level of pollutants and deterioration in air quality. There have been various studies that relate human activities to changes in atmospheric composition [12,13]. China is one of the most populous countries in the world, with rapid strides in urbanization, industrialization and commercial growth. These developments have strong impacts on air quality and most of the Chinese cities are severely impacted. Studies over various cities in China showed that a clear decline in pollutant concentration is observed when human activities are limited, especially during the annual Spring Festival [14–17]. Several studies showed that controlled emissions and reduction in anthropogenic activities during special case instances considerably improved the air quality and tropospheric trace gas concentration. The instances reported in the literature include the China Victory Day parade (2015), the Youth Olympic Games in Nanjing (2014), the Asian Pacific Economic Cooperation Conference (APEC, 2014), the Guangzhou Asian Games (2010) and the Beijing Olympics (2008) [18–22]. The end of 2019 marked the emergence of a novel coronavirus in the Chinese city of Wuhan, recognized as SARS CoV-2, and the resulting disease was termed as COVID-19. Following the COVID-19 pandemic, the Chinese government took substantial lockdown measures to reduce mobility and activity in order to stop the spread of the virus. Studies over various parts of the world to elucidate the influence of COVID-19 lockdowns on regional emissions and atmospheric quality reported reductions in the levels of most important criteria pollutants in the atmosphere [23–28].

The prime objective of the study is to outline the influence of restricted human activity on two criteria pollutants (NO<sub>2</sub> and HCHO) over Shanghai, China. The study also takes into account the meteorological conditions and regional transport using the Hybrid Single-Particle Lagrangian Integrated Trajectory (HYSPLIT) model in order to get a better understanding of the events. The observations were made by the multi-axis differential optical absorption spectroscope (MAX-DOAS) instrument which employs the powerful differential optical absorption spectroscopy (DOAS) technique to provide valued data for aerosols and trace gases in the atmosphere [29]. Owing to its simplicity and cost-effectiveness, MAX-DOAS has extensively been used for atmospheric monitoring over the past decades [30–33]. For the current study, off-axis measurements from the ground-based observations from January to April 2019 and 2020 were analyzed over Shanghai using the data from the MAX-DOAS instrument. The impact of Spring Festival holidays on regional emissions and pollutant concentrations was analyzed by categorizing the study period into

three distinct phases (pre-Spring Festival, Spring Festival and post-Spring Festival) while taking into account the meteorological conditions over the study period for 2019 and 2020. Further, the change in vertical column densities (VCDs) during the COVID-19 lockdown was examined.

## 2. Materials and Methods

### 2.1. Observation Site

The MAX-DOAS instrument was fixed on the Environmental Science Building at Fudan University Jiangwan Campus (31.34° N, 121.52° E) at an elevation of about 21 m above sea level. It is located in Yangpu District in Shanghai which is one of the direct administered metropolises of the People's Republic of China. The city is located on the Southern estuary of the Yangtze River. As of 2019, the population of Shanghai was about 24.28 million, which makes it the biggest city in China in terms of population and the second largest in the world. The city is the epicenter for finance, manufacturing, research, industry and technology. Shanghai has the world's most active container port. Figure 1 shows the study site.

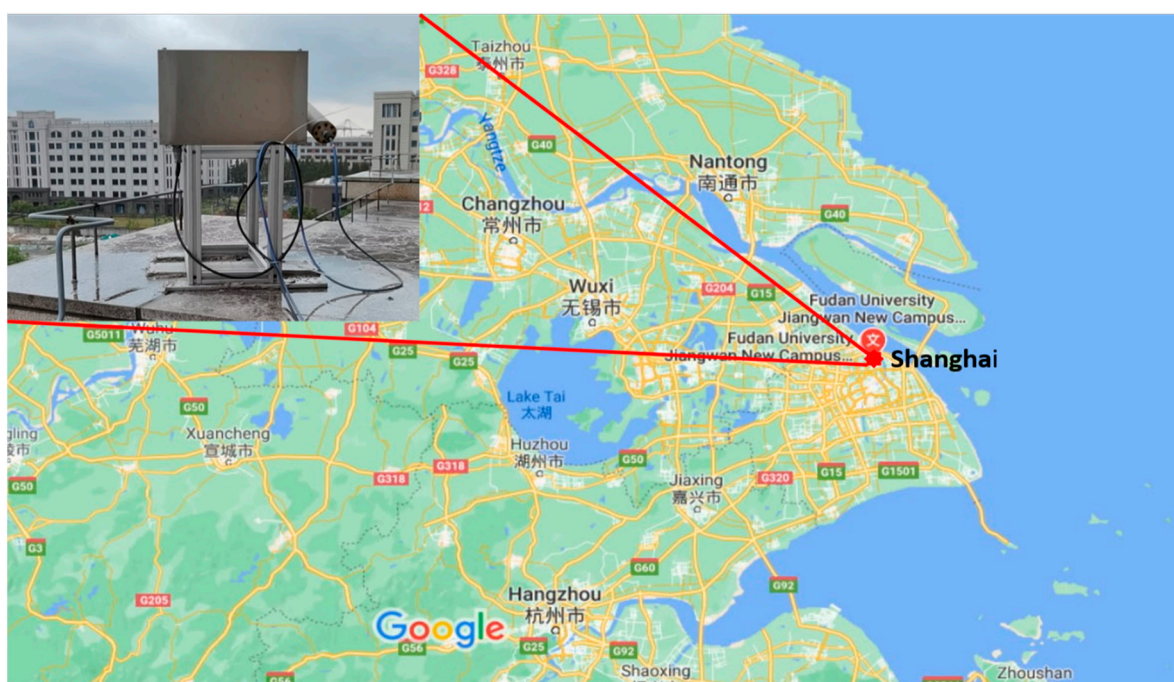


**Figure 1.** Multi-axis differential optical absorption spectroscopy (MAX-DOAS) observation site at Fudan University, Yangpu District, Shanghai (Map Source: Google Map).

### 2.2. MAX-DOAS Instrument

The MAX-DOAS apparatus mainly consists of a scanning telescope controlled by a stepping motor, a spectrometer (Ocean Optics, QE65 Pro) and a computer system [34,35]. The spectrometer, equipped with a charge-coupled device (CCD) detector (1044 horizontal  $\times$  64 vertical, cooling to  $-15^{\circ}\text{C}$ ), is used to measure spectra in the wavelength range from 296 to 480 nm with a spectral resolution of 0.5 nm full width half maximum (FWHM). The telescope was pointed north. The scanning sequence of the telescope consists of ten elevation viewing angles (EVA), i.e.,  $2^{\circ}$ ,  $3^{\circ}$ ,  $5^{\circ}$ ,  $7^{\circ}$ ,  $10^{\circ}$ ,  $15^{\circ}$ ,  $20^{\circ}$ ,  $30^{\circ}$ ,  $45^{\circ}$  and  $90^{\circ}$ , which takes about 10 minutes for each cycle. The signal of the dark current was extracted automatically from background measurements taken each night.

### 2.3. DOAS Analysis

Accurate column measurements for the trace gases in the atmosphere are possible only because the MAX-DOAS instrument can measure dispersed sunlight at several elevations known as EVA. Zenith measurements were selected as the Fraunhofer reference spectrum for each measurement sequence which was then subtracted from the off-zenith spectrum to obtain differential slant column densities (DSCDs), thereby minimizing the stratospheric interference to the tropospheric measurements [1]. QDOAS software v. 3.2 developed by BIRA-IASB (<http://uv-vis.aeronomie.be/software/QDOAS/>) was used to analyze the spectra [36]. Table 1 describes the settings for NO<sub>2</sub> and HCHO retrieval from DOAS, where “parameters” refers to the absorption cross-sections of interfering compounds and “data source” refers to the source and temperature at which absorption cross-sections are measured. A high-resolution solar spectrum was used to calibrate the wavelength [37].

**Table 1.** Detailed settings for NO<sub>2</sub> and HCHO retrieval from differential optical absorption spectroscopy.

Parameters	Data Source	Trace Gases	
		NO <sub>2</sub>	HCHO
Wavelength (nm)		337–370	325–350
HCHO	297 K, [38]	✓	✓
SO <sub>2</sub>	298 K, [39]	X	✓
NO <sub>2</sub>	220 K, [39]	✓	✓
NO <sub>2</sub>	298 K, [39]	✓	✓
BrO	223 K, [40]	✓	X
O <sub>3</sub>	223 K, [40]	✓	✓
O <sub>3</sub>	243 K, [41]	✓	X
O <sub>4</sub>	293 K, [42]	✓	✓
Ring	Calculated with QDOAS	✓	✓
Polynomial degree		5	5

Owing to the scattering processes in the atmosphere, the quality of data is likely to be impacted. To avoid this, certain filters are applied to ensure quality. The data with a root mean square (RMS) greater than 0.002 and a solar zenith angle greater than 75 were filtered out for this study. The RMS represents the average error in spectral analysis for MAX-DOAS. Figure 2 shows a typical fitting spectrum for DOAS at an elevation viewing angle of 30° over Shanghai.

Differential air mass factors (DAMFs) were used for the calculation of tropospheric vertical column density (VCD<sub>trop</sub>) [43,44].

$$\text{VCD}_{\text{trop}} = \frac{\text{DSCD}_{\alpha}}{\text{DAMF}_{\alpha}} \quad (1)$$

Here,  $\alpha$  represents the angle at which consequent observations are made, whereas the following equation gives the DAMF:

$$\text{DAMF}_{\alpha} = \text{AMF}_{\alpha} - \text{AMF}_{90^{\circ}} \quad (2)$$

$$\text{VCD}_{\text{trop}} = \frac{\text{DSCD}_{\alpha}}{(\text{AMF}_{\alpha} - \text{AMF}_{90^{\circ}})} \quad (3)$$

The AMF is calculated using geometric approximation [45].

$$\text{AMF} = \frac{1}{\sin \alpha} \quad (4)$$

Equation (3) now implies

$$\text{VCD}_{\text{trop}} = \frac{\text{DSCD}_{\alpha}}{1/\sin \alpha - 1} \quad (5)$$

Despite the fact that this is used as a standard method, a few uncertainties related to it exist, especially when elevation angles are lower [1].

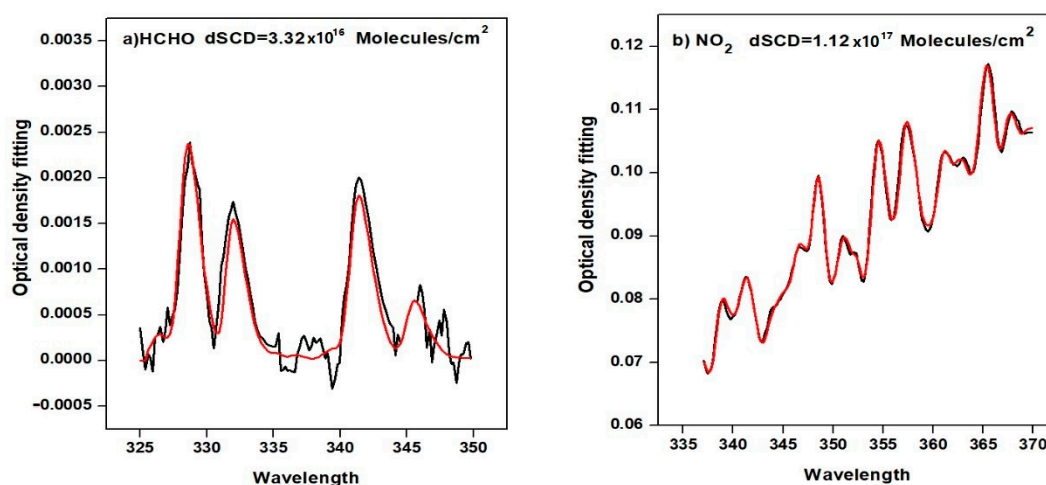


**Figure 2.** Typical DOAS fit for formaldehyde (HCHO) and nitrogen dioxide (NO<sub>2</sub>) at 30° elevation angle on 01 January 2020 over Shanghai. Fitted optical densities are represented by the red line, while measured densities are denoted by the black line.

#### 2.4. Ancillary Data

In situ measurements for the criteria pollutants including NO<sub>2</sub>, O<sub>3</sub>, AQI and PM<sub>2.5</sub> were downloaded (available online: <https://www.aqistudy.cn/>, last accessed on 27 September 2020). The daily mean concentration of these measurements spanning from January to April 2019 and 2020 was used in this study. ERA5 reanalysis data for meteorological parameters over Shanghai were obtained from the Copernicus Data Hub (available online: <https://cds.climate.copernicus.eu>, last accessed on 14 October 2020).

#### 2.5. Backward Trajectory Modeling

The Hybrid Single-Particle Lagrangian Integrated Trajectory (HYSPLIT) model used to investigate the transportation of pollutants over Shanghai was developed by the National Oceanic and Atmospheric Administration Air Resources Laboratory (NOAA ARL) [46] (<https://www.arl.noaa.gov/hysplit/>, last accessed: 15 December 2020). The trajectory simulation used meteorological data from the Global Data Assimilation System (GDAS) (24 vertical levels; spatial resolution of 0.5° × 0.5°). Air masses arriving at the observation site were used to compute backward trajectories. This part mainly aims to study the effect of regional transport on pollutants. The transport in the lower atmosphere is easily restricted by the underlying surface. The height of 500 m above ground level (AGL) for the model run was selected to show well-mixed conditions in the atmospheric boundary layer which are likely to affect the surface air quality.

### 3. Results

#### 3.1. Overview of the Observations

The MAX-DOAS and in situ measurements for this study span from January to April for 2019 and 2020. MAX-DOAS observations were conducted for NO<sub>2</sub> and HCHO, while in situ measurements were obtained for NO<sub>2</sub>, PM<sub>2.5</sub>, O<sub>3</sub> and AQI. MAX-DOAS average NO<sub>2</sub> VCDs for the study period were  $1.15 \times 10^{17}$  and  $1.13 \times 10^{17}$  molecules/cm<sup>2</sup>, while mean HCHO VCDs were  $3.17 \times 10^{16}$  and  $2.57 \times 10^{16}$  molecules/cm<sup>2</sup> during 2019 and 2020, respectively. The time series of daily mean VCDs for NO<sub>2</sub> and HCHO over the study period are shown in Figure 3.

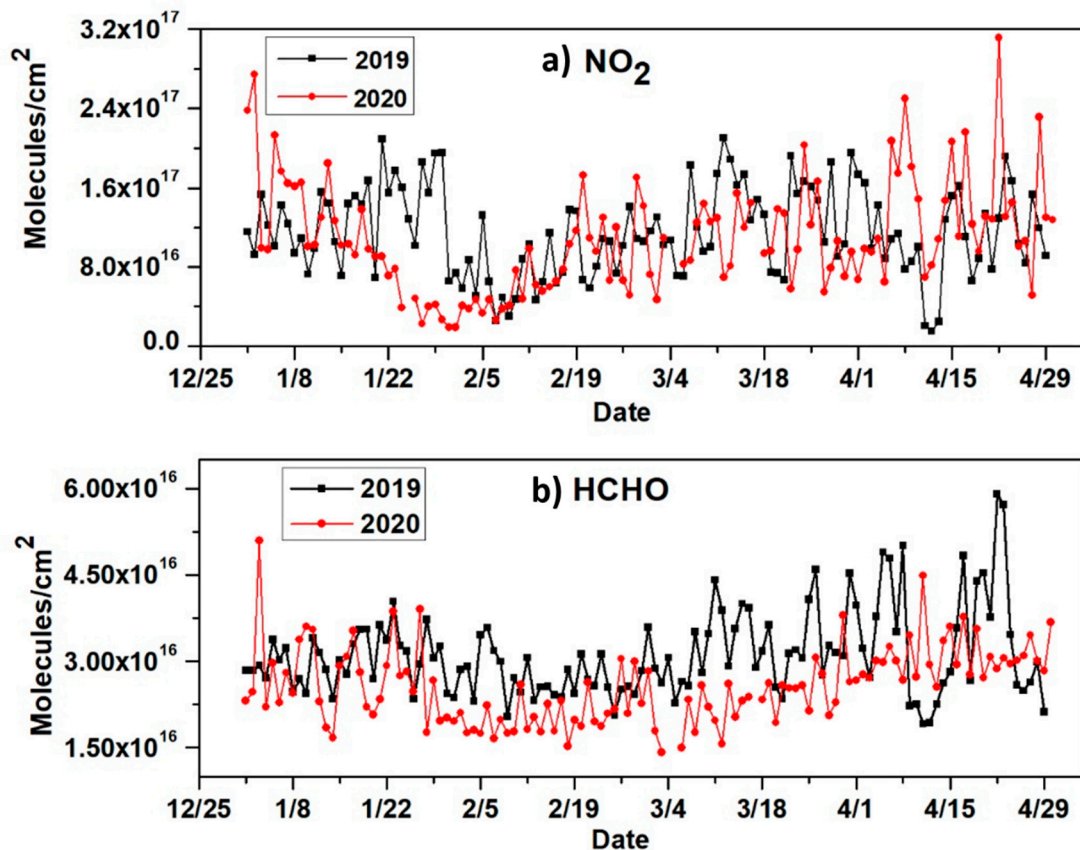


**Figure 3.** Time series for (a) nitrogen dioxide (NO<sub>2</sub>) and (b) formaldehyde (HCHO) vertical column densities (VCDs) from January to April 2019 and 2020 obtained from MAX-DOAS at 30° elevation viewing angle over Shanghai.

Time series were also generated using daily mean in situ measurements for NO<sub>2</sub>, PM<sub>2.5</sub> and the air quality index (AQI). Based on the ambient pollutants, the AQI quantifies the overall quality of the air over the monitored area. Equation (6) gives the formula by which the AQI is calculated.

$$\text{AQI} = \max\{\text{IAQI1}, \text{IAQI2}, \text{IAQI3}, \dots, \text{IAQIn}\} \quad (6)$$

Here, AQI stands for air quality index; IAQI refers to the individual air quality index, which includes the air pollutants; and n is the number of ambient air pollutants. The AQI used in this study is calculated based on six ambient pollutants, nitrogen dioxide (NO<sub>2</sub>), sulfur dioxide (SO<sub>2</sub>), ozone (O<sub>3</sub>), carbon monoxide (CO), PM<sub>10</sub> and PM<sub>2.5</sub> [47]. Figure 4 shows the daily mean concentration of these atmospheric species for the study span.

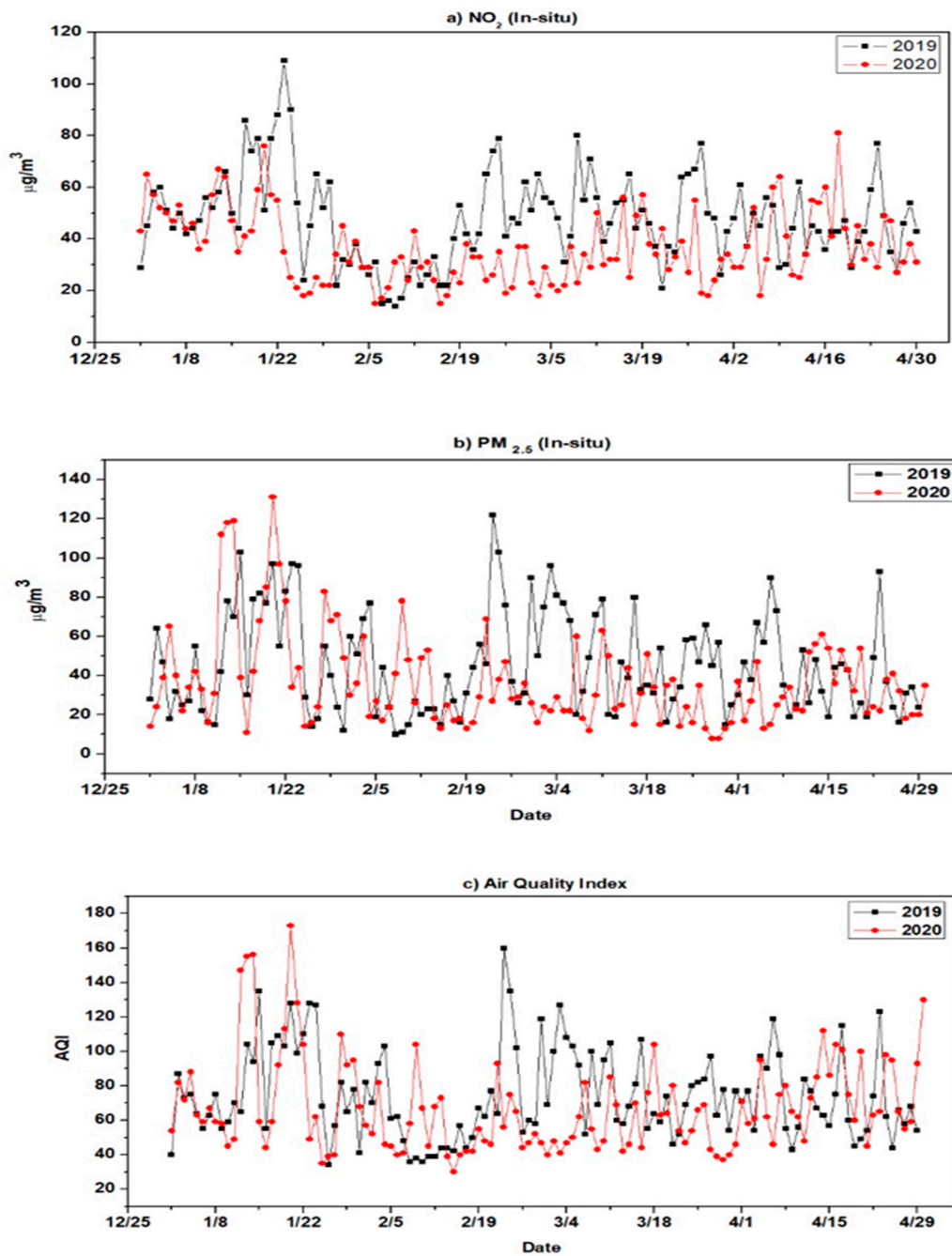


**Figure 4.** Time series of in situ measurements for (a) nitrogen dioxide ( $\text{NO}_2$ ), (b) particulate matter ( $\text{PM}_{2.5}$ ) and (c) the air quality index (AQI) over the study area from January to April during 2019 and 2020.

The aerosol and trace gas distribution along with the residence time and chemical behavior is largely affected by the meteorological settings over the vicinity [1,2]. Temperature and wind speed are of pivotal significance in determining the trace gas concentrations. Table 2 shows the average temperature, wind speed and pressure for the study period during 2019 and 2020 along with the respective standard deviations over Shanghai. It is to be noted here that these are the grid values and not the measurements and as Shanghai lies near the coast, small standard deviations may be linked to the coarse resolution of ERA5.

**Table 2.** Changes in meteorological parameters over Shanghai.

Parameter	2019 (Avg $\pm$ Std)	2020 (Avg $\pm$ Std)
Temperature/ $^{\circ}$ C	10.3 $\pm$ 5.2	10.9 $\pm$ 4.8
Wind Speed/ $\text{m}\cdot\text{s}^{-1}$	3.5 $\pm$ 1.4	3.7 $\pm$ 1.6
Pressure/hPa	1021.3 $\pm$ 7.1	1021.8 $\pm$ 5.4

The box plot for the average temperature and windspeed over the study period is shown in Figure 5. It is evident from the figure that there was no significant change in meteorological parameters during 2020 compared to the previous year.

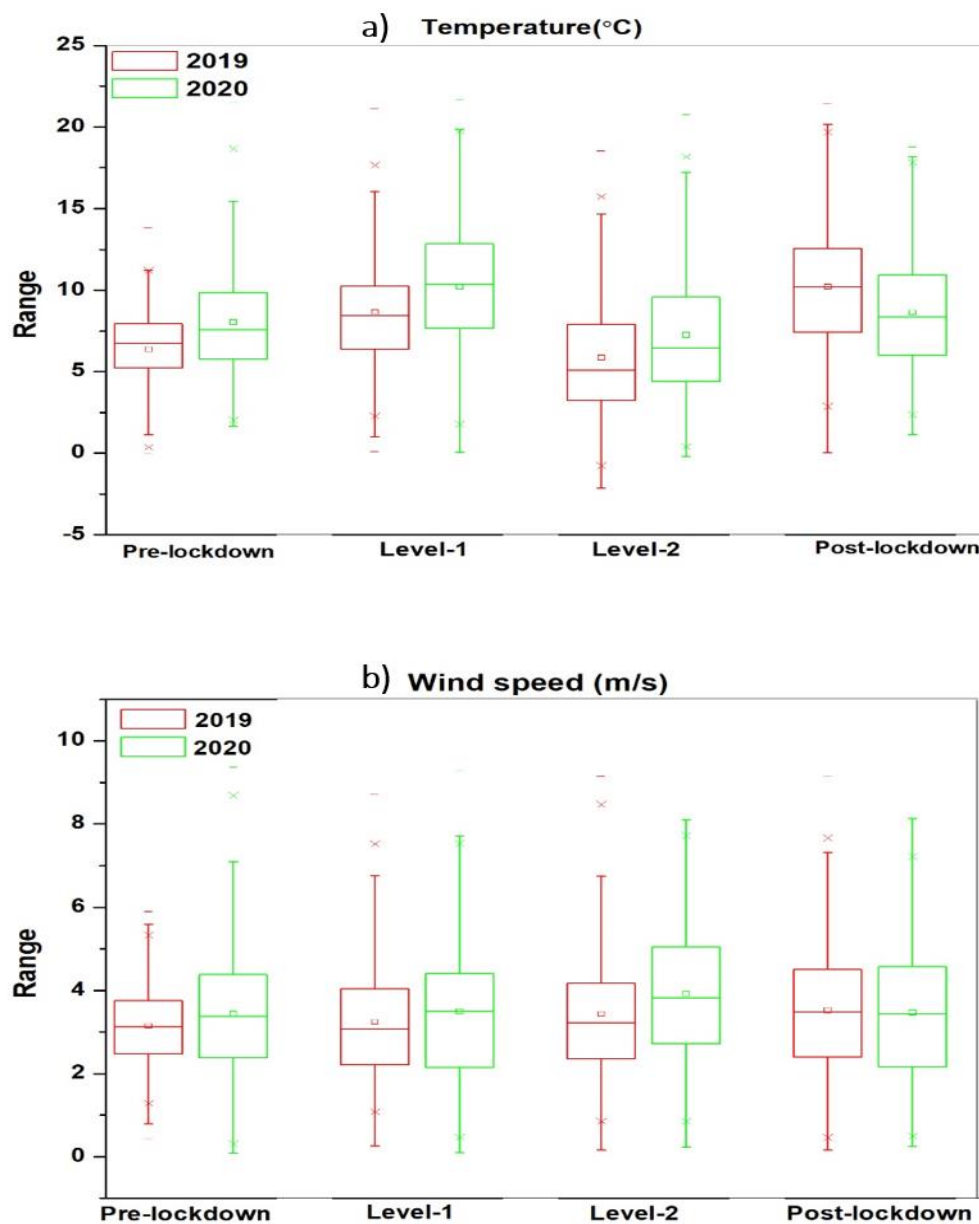


**Figure 5.** The boxplot categorized into four levels of the study period for (a) temperature ( $^{\circ}$ C) and (b) windspeed (m/s) attained from ERA5.

### 3.2. Impact of COVID-19 Lockdown

During the lockdown, strict measures were adopted at Level-1 (first level of emergency response), while somewhat relaxed measures were taken during Level-2 (second level of emergency response). To understand the changes in air quality owing to the lockdown, the study span was divided into four stages: pre-lockdown (1 January–23 January), Level-1 (24 January–26 February), Level-2 (27 February–31 March) and post-lockdown (1 April–30 April). In order to make comparisons, same days in 2019 were categorized similarly despite the fact that no lockdown occurred during the previous year. Overall, the change in VCDs during the lockdown periods is depicted in Table 3 in terms of percentage, where the negative sign indicates a reduction. It is worth mentioning here that the change during Level-1 and Level-2 is calculated by keeping pre-lockdown levels as the reference.

**Table 3.** Percentage change in mean VCDs of HCHO and NO<sub>2</sub> for Level-1 and Level-2 of the lockdown for 2020 and corresponding days in 2019.

Species	Instrument	Year	Level-1	Level-2
NO <sub>2</sub>	MAX-DOAS	2019	−24%	1%
		2020	−43%	−20%
HCHO	MAX-DOAS	2019	−6.62%	+2%
		2020	−24%	−22%

It is evident from Table 3 that the mean VCDs during Level-1 and Level -2 were considerably lower during 2020 as compared to 2019. The reduction in mean VCDs during Level-1 for 2019 was observed under the no lockdown scenario which can be attributed to annual Spring Festival holidays and is discussed in detail under Section 3.3. Figure 6 shows the box plot for NO<sub>2</sub> and HCHO VCDs from the MAX-DOAS observations over the locality.

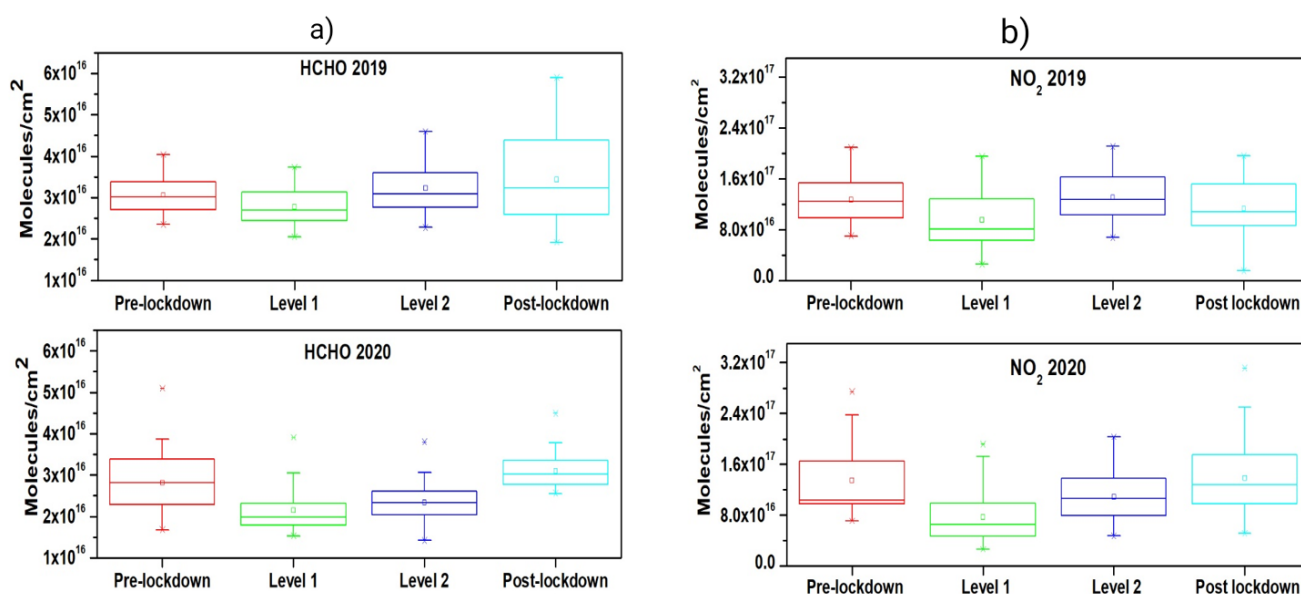


**Figure 6.** The boxplot categorized into four levels of the study period for (a) formaldehyde (HCHO) and (b) nitrogen dioxide (NO<sub>2</sub>) vertical column densities (VCDs) attained from the MAX-DOAS instrument.

### Weekly Cycle

As human activities are broadly categorized according to a weekly cycle, it is very important to check the effect of weekly cycles on anthropogenic emissions. Human activities over the week are high during the working days, while they decline over the weekends [48].

This is termed as the weekend effect. Figure 7 shows the weekly cycles of  $\text{NO}_2$  and HCHO observed over Shanghai for normal days and the lockdown days.

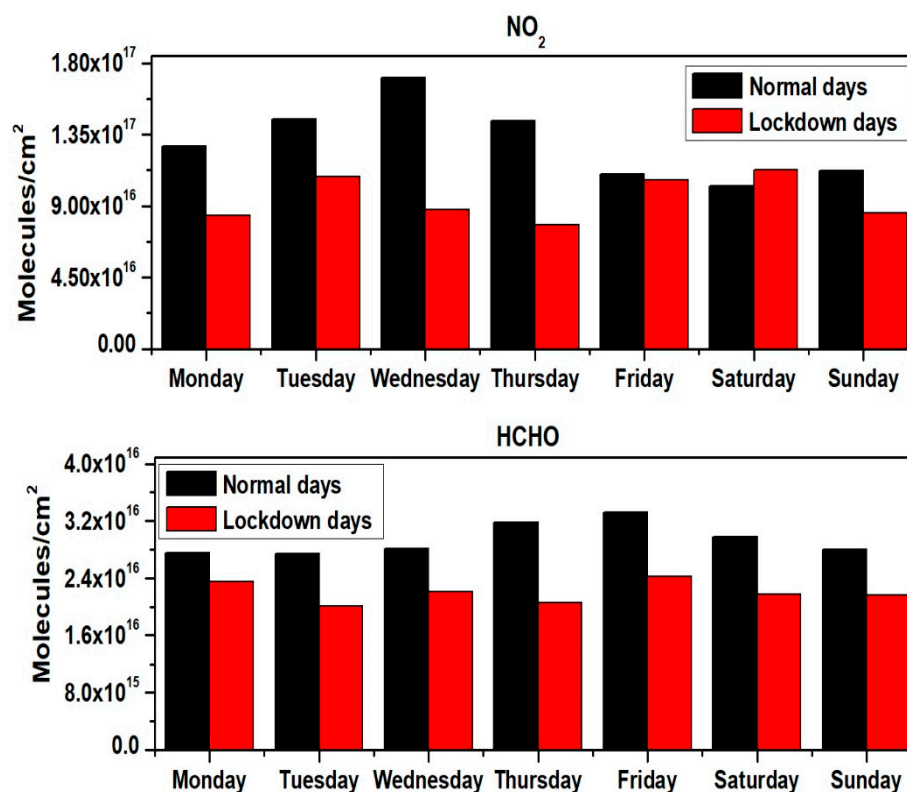


Figure 7. Weekly cycles of nitrogen dioxide ( $\text{NO}_2$ ) and formaldehyde (HCHO) vertical column densities (VCDs) observed over Shanghai for normal days as compared to the lockdown period.

Figure 7 shows that the average daily mean VCDs were higher for normal days compared to the lockdown days. It is also evident that the variation in daily mean VCDs for different days of the week during the lockdown is very low, giving no definite weekend effect compared to the normal days when a normal weekly cycle is observed.

### 3.3. Spring Festival and Regional Transport

To compare the impact of the Spring Festival on the atmospheric concentration of  $\text{NO}_2$  and HCHO for 2019 and 2020, we categorized the observations into three phases each equal to the number of the Spring Festival holidays: pre-Spring Festival, Spring Festival and post-Spring Festival. The exact categorization and dates are mentioned in Table 4.

Table 4. Spring festival study period for 2019 and 2020.

Year	Pre-Spring Festival	Spring Festival	Post-Spring Festival
2019	28 January–3 February	4 February–10 February	11 February–17 February
2020	18 January–24 January	25 January–31 January	1 February–7 February

Figure 8 shows the time series of  $\text{NO}_2$  and HCHO VCDs as measured by the observations from the MAX-DOAS during and around the annual Spring Festival for 2019 and 2020. The gray region in the figure specifies the Spring Festival period.

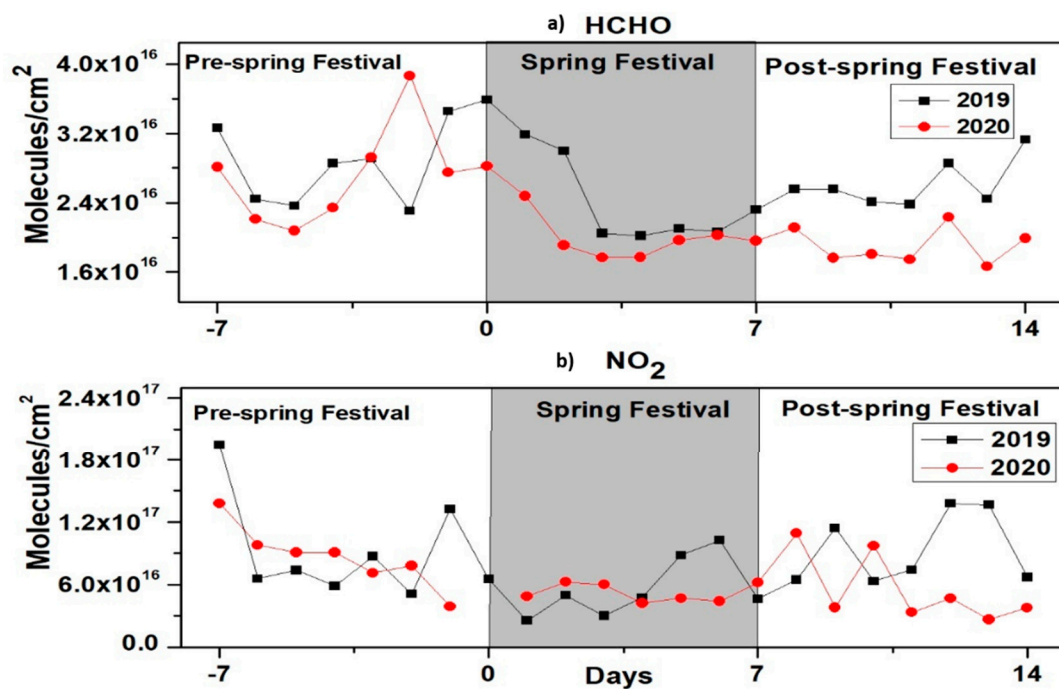


**Figure 8.** Impact of Spring Festival holidays on the vertical column densities (VCDs) of (a) nitrogen dioxide ( $\text{NO}_2$ ) and (b) formaldehyde (HCHO) over Shanghai.

Backward trajectories modeled for the study period are shown in Figure 9. The target point for the trajectories was set at Fudan University, Shanghai, at a height of approximately 500 m. This part mainly aims to study the effect of regional transport on pollutants. The transport in the lower atmosphere is easily restricted by the underlying surface. The height of 500 m above ground level (AGL) for the model run was selected to show well-mixed conditions in the atmospheric boundary layer which are likely to affect the surface air quality.

Each line in the figure represents the air mass trajectory for the past 24 h with one point representing one hour. The trajectories indicate a similar pattern for 2019 pre- and post-Spring Festival holidays, while different air mass transportation was observed during Spring Festival holidays. On the other hand, for 2020, the Spring Festival and post-Spring Festival days indicate similar transportation conditions, while the pre-Spring Festival days depict a different pattern. After the Spring Festival in 2019 and 2020, major air masses appear to be coming from the sea which may carry a low concentration of pollutants. As there are more air masses from inland before the Spring Festival, the high VCDs of HCHO and  $\text{NO}_2$  in Shanghai may be affected by this transmission.

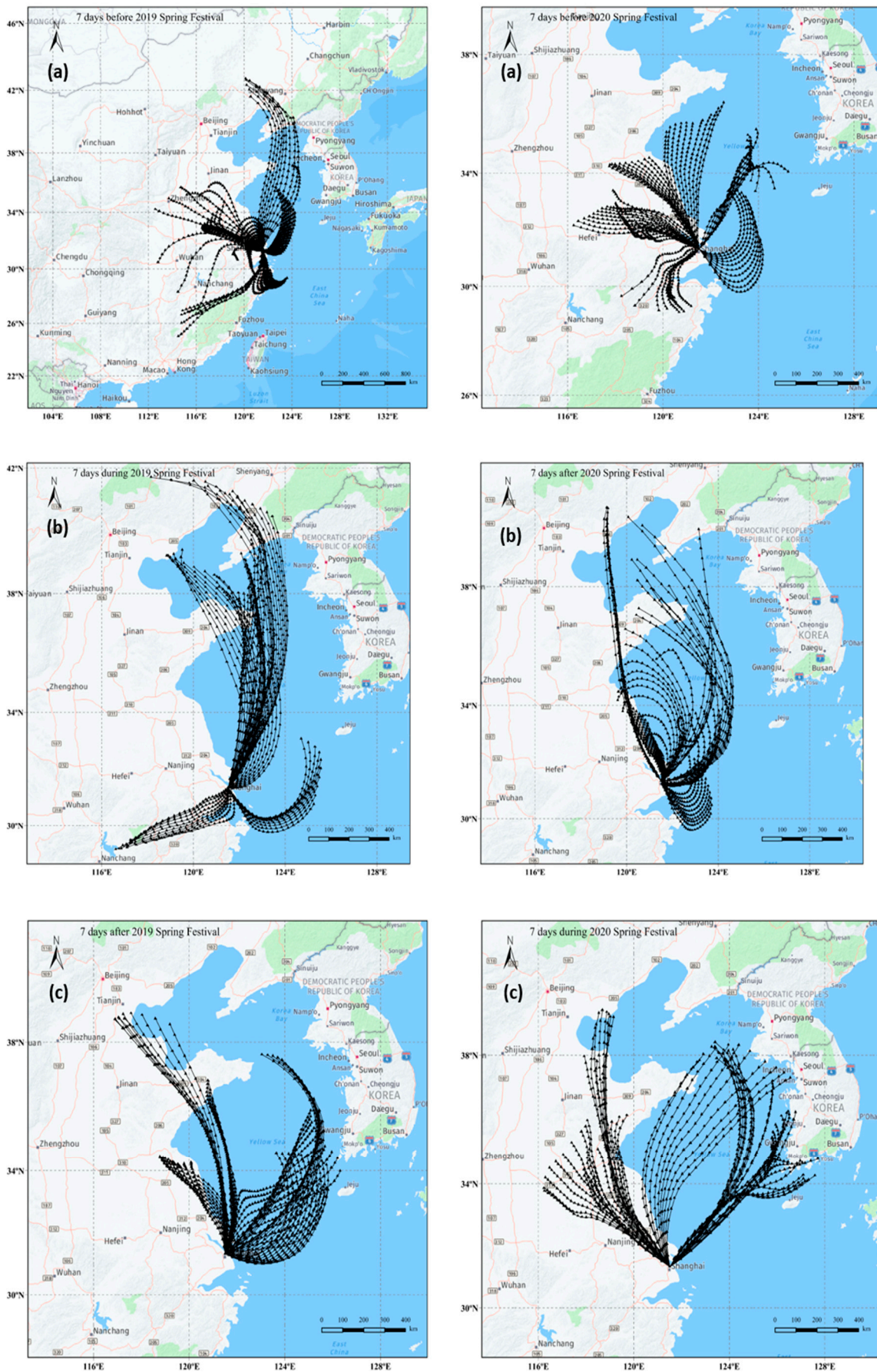
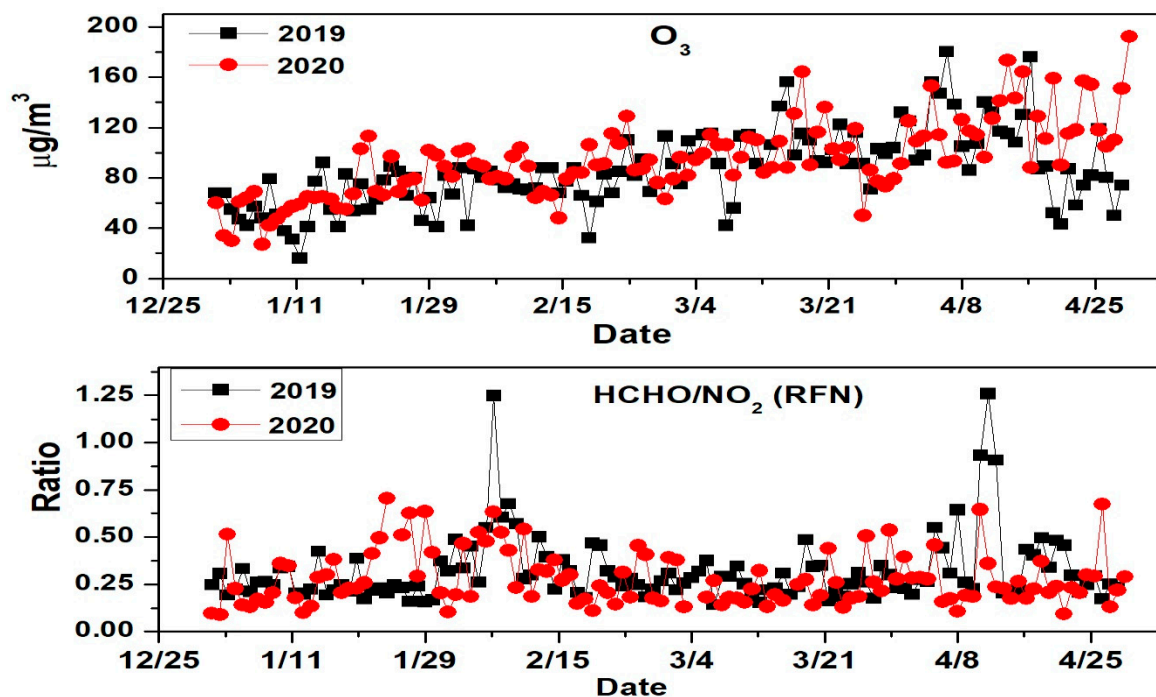


Figure 9. Clusters of backward trajectories (a) before, (b) during and (c) after the Spring Festival, 2019 and 2020.

### 3.4. Trends in Ozone ( $O_3$ ) Concentration

In situ measurements show that the  $O_3$  concentration remained unaffected by the lockdown events and continued to grow steadily over the study period, as shown in Figure 10. The formation of tropospheric  $O_3$  via photochemical reactions is largely impacted by VOCs and oxides of nitrogen in the atmosphere [49]. Therefore, it is essentially important to control the level of  $NO_x$  and VOCs to limit  $O_3$  production.  $O_3$  production can either be  $NO_x$ -limited or VOC-limited depending on which species is in excess. As HCHO comes as the oxidation product from a variety of VOCs, it is used as a proxy for the VOCs reactivity [50]. To investigate the trend of  $O_3$  over the study period, the ratio of HCHO to  $NO_2$  VCDs (RFN) was calculated over Shanghai. Three distinct regions were defined in the literature to describe the linkage of RFN and  $O_3$  formation: when the RFN is lower than 1,  $O_3$  production is VOC-limited; when the RFN is greater than 2,  $O_3$  production is  $NO_x$ -limited; and when the RFN lies between 1 and 2,  $O_3$  production lies in a transition regime where both  $NO_x$  and VOC may affect  $O_3$  production [51]. Here, the ratio of HCHO to  $NO_2$  used to analyze  $O_3$  sensitivity falls in the VOC-limited regime and is depicted in Figure 10 for the study period.



**Figure 10.** Ozone ( $O_3$ ) measurements over Shanghai for the study period. Daily averaged HCHO/ $NO_2$  ratio (RFN) at Shanghai.

## 4. Discussion

Meteorological conditions significantly impact the chemical behavior and residence time of trace gas species in the lower atmosphere, thereby affecting the pollutant distribution over the locality. Substantial evidence exists concerning the significance of meteorological factors on the distribution of aerosol and trace gases in the atmosphere [14,52]. To have an improved understanding of the sources and sinks of atmospheric pollutants and their dependence on certain meteorological parameters, it is pivotal to have a multidimensional and dynamic picture of the atmosphere by looking at the overall tropospheric profile. Meteorological conditions for the study period remain the same on average for 2019 and 2020. The meteorology results obtained from ERA5 are gridded values which might have caused uncertainties in the analysis. Therefore, the impact of these conditions on the atmospheric concentration of trace gases during the lockdown period is not pronounced. Similar results were reported in the literature [53].

The lockdown period to contain COVID-19 and the Spring Festival were taken into account assuming that the reduction in overall mobility and shutting down of industry, offices and institutions, thereby reducing the anthropogenic activity, are likely to impact the overall daily mean concentration of trace gas species in the atmosphere. Several studies have been conducted across the world to elucidate the influence of COVID-19 lockdowns on trace gas concentrations and tropospheric distribution. The results reported in this study comply with those studies reporting an overall decline in trace gas concentration during lockdown periods. NO<sub>2</sub> VCDs showed a decline following the start of lockdown in 2020. However, in 2019, the reduction in emissions was observed after the start of the annual Spring Festival. Similar trends were observed for HCHO during the same period. Recent studies carried out over various parts of the world show similar trends [23–28,52]. Our results show higher reduction in the NO<sub>2</sub> VCDs as compared to HCHO, owing to the fact that NO<sub>2</sub> mainly comes from anthropogenic sources. Therefore, the reduction in NO<sub>2</sub> VCDs was more pronounced during the lockdown with the closure of businesses, industry, transportation and economic activities. A comparison of in situ measurements of NO<sub>2</sub> showed a reduction in the concentration of trace gas species during the lockdown period as well as the corresponding Spring Festival holidays of the previous year, which complies with the trends observed by the MAX-DOAS measurements. PM<sub>2.5</sub> levels dropped in the corresponding phases with an improvement in the AQI of the city. An improvement in the AQI and a reduction in PM<sub>2.5</sub> during the lockdown period have been reported in the literature [52–56]. Level-1 of the lockdown depicted the highest reduction in the concentration of NO<sub>2</sub>, HCHO and PM<sub>2.5</sub> and the AQI during 2020 as compared to 2019. The weekly cycle showed that the VCDs of NO<sub>2</sub> were considerably lower for the lockdown days compared to normal days during the week, while for weekends, the observed VCDs were almost equal for normal and lockdown days. For HCHO, a definite pattern exists over the week for normal days, while considerably lower values and a linear trend were observed during the lockdown. This can be accredited to the fact that every day of the week had almost the same anthropogenic activity during the lockdown. Anthropogenic activities are considered as a secondary source of HCHO, while biogenic emissions are the primary sources. Therefore, with reduced anthropogenic activity, biogenic emissions became the only constant source of HCHO, leading to uniform VCDs throughout the week. Overall, the variation in daily mean VCDs of NO<sub>2</sub> and HCHO for different days of the week was non-significant for the lockdown period, giving no definite weekly cycle.

The data from the Ministry of Transport show an almost 50% reduction in traffic load for the 2020 annual Spring Festival as compared to the previous year (available online: <http://www.mot.gov.cn/>, accessed on 22 June 2020). Several studies report the impact of Spring Festival holidays on the trace gas concentration in the atmosphere [14–17]. Our results comply with the literature, showing that the trace gas VCDs reduced significantly during the annual Spring Festival for 2019 and 2020 with average low values during 2020 as compared to 2019. The backward trajectories generated for and around the Spring Festival days showed that more air masses were coming from the sea during and after the Spring Festival in 2020 which may carry less pollutant load, while for 2019, more inland transmission happened during the Spring Festival holidays. This needs to be studied further in order to obtain a clearer picture of the impact of long-range transport.

The O<sub>3</sub> concentration did not show any impact of the lockdown and continued to grow steadily over the study period with the intensification of solar radiation during late winter and early spring. The observed value of the RFN used for the sensitivity analysis of tropospheric O<sub>3</sub> formation to the precursor species (NO<sub>x</sub> and VOCs) depicts that O<sub>3</sub> production over the study area is mostly VOC-limited. Nevertheless, the subject needs further investigation. Due to the specific nature of events, different studies reported the effects of COVID-19 lockdowns on air quality and trace gas concentrations. Our results comply with recent studies depicting an overall decline in trace gas concentrations and an improvement in air quality [23–28,53–57].

## 5. Conclusions

The average VCDs of NO<sub>2</sub> and HCHO as observed from the MAX-DOAS instrument were lower in 2020 compared to same days in 2019. In situ measurements for NO<sub>2</sub>, PM<sub>2.5</sub> and the AQI portrayed similar results, while the meteorological conditions remained similar for both the years. During the COVID-19 lockdown in 2020, the reduction in NO<sub>2</sub> and HCHO VCDs was observed to be 43% and 24% for Level-1 and 20% and 22% for Level-2, respectively. Meanwhile, no lockdown happened during 2019, but the VCD of NO<sub>2</sub> and HCHO showed a decline of 24% and 6.64%, respectively, for the period categorized as Level-1, while a small rise was observed during Level-2. The reduction in atmospheric VCDs during Level-1 in 2019 is attributed to the annual Spring Festival holidays. Further, the comparison of weekly cycles for normal days with lockdown days showed that the variation between atmospheric VCDs of NO<sub>2</sub> and HCHO on different days of the week is non-significant for the lockdown days, thereby depicting no definite weekly cycle. The VCDs of HCHO and NO<sub>2</sub> showed a drop during the annual Spring Festival holidays for 2019 as well as 2020. However, the post-Spring Festival days showed a rise in the VCDs of observed trace gases for 2019, while they dropped further for 2020, which is attributed to the COVID-19 lockdown. Backward trajectories showed that major air masses were coming from the sea after the Spring Festival for 2019 and 2020, which can be attributed to the smaller pollutant load during that period. However, this needs to be studied further in order to get a better understanding. In situ measurements for the levels of O<sub>3</sub> showed no impact of the lockdown on the tropospheric concentration of O<sub>3</sub> which continued to grow steadily from January to April in 2019 as well as 2020. The ratio of HCHO to NO<sub>2</sub> (RFN) depicted that O<sub>3</sub> production mostly fell in the VOC-limited regime.

**Author Contributions:** Conceptualization, Z.B. and A.T.; methodology, A.T. and Z.J. (Zhu Jian); software, S.Z. and A.T.; validation, Z.J. (Zhu Jian), R.X. and S.W.; formal analysis, A.T.; investigation, S.W.; resources, Z.B.; data curation, A.T.; writing—original draft preparation, A.T. and Z.J. (Zeeshan Javed); writing—review and editing, Z.B. and M.B.; visualization, Z.J. (Zhu Jian); supervision, Z.B. and S.W.; project administration, Z.B.; funding acquisition, Z.B. All authors have read and agreed to the published version of the manuscript.

**Funding:** This research was funded by the National Key Research and Development Program of China 2017YFC0210002, the National Natural Science Foundation of China (21777026, 41775113, 21976031, 42075097).

**Institutional Review Board Statement:** Not applicable.

**Informed Consent Statement:** Not applicable.

**Data Availability Statement:** The data presented in this study are available on request from the corresponding author.

**Acknowledgments:** The authors would also like to thank the National Oceanic and Atmospheric Administration (NOAA) Air Resources Laboratory (ARL) for the provision of the HYSPLIT transport and dispersion model used in this publication.

**Conflicts of Interest:** The authors declare no conflict of interest.

## References

1. Javed, Z.; Liu, C.; Khokhar, M.F.; Tan, W.; Liu, H.; Xing, C.; Ji, X.; Tanvir, A.; Hong, Q.; Sandhu, O.; et al. Ground-based MAX-DOAS observations of CHOCHO and HCHO in Beijing and Baoding, China. *Remote Sens.* **2019**, *11*, 1524. [[CrossRef](#)]
2. Javed, Z.; Liu, C.; Ullah, K.; Tan, W.; Xing, C.; Liu, H. Investigating the effect of different meteorological conditions on MAX-DOAS observations of NO<sub>2</sub> and CHOCHO in Hefei, China. *Atmosphere* **2019**, *10*, 353. [[CrossRef](#)]
3. Crutzen, P.J. The role of NO and NO<sub>2</sub> in the chemistry of the troposphere and stratosphere. *Annu. Rev. Earth Planet Sci.* **1979**, *7*, 443–472. [[CrossRef](#)]
4. Crutzen, P.J. The influence of nitrogen oxides on the atmospheric ozone content. *Q. J. R. Meteorol. Soc.* **1970**, *96*, 320–325. [[CrossRef](#)]
5. Jang, M.; Kamens, R.M. Characterization of secondary organic aerosol from the photooxidation of toluene in the presence of NO<sub>x</sub> and 1-propene. *Environ. Sci. Technol.* **2001**, *35*, 3626–3639. [[CrossRef](#)]

6. Finlayson-Pitts, B.J.; Pitts, J.N. *Chemistry of the Upper and Lower Atmosphere: Theory, Experiments and Applications*; Academic Press: San Diego, CA, USA, 2000.
7. Delmas, R.; Serça, D.; Jambert, C. Global inventory of NO<sub>x</sub> sources. *Nutr. Cycl. Agroecosyst.* **1997**, *48*, 51–60. [[CrossRef](#)]
8. Beirle, S.; Boersma, K.F.; Platt, U.; Lawrence, M.G.; Wagner, T. Megacity emissions and lifetimes of nitrogen oxides probed from space. *Science* **2011**, *333*, 1737–1739. [[CrossRef](#)]
9. Schreier, S.F.; Richter, A.; Peters, E.; Ostendorf, M.; Schmalwieser, A.W.; Weihs, P.; Burrows, J.P. Dual ground-based MAX-DOAS observations in Vienna, Austria: Evaluation of horizontal and temporal NO<sub>2</sub>, HCHO, and CHOCHO distributions and comparison with independent data sets. *Atmos. Environ. X* **2020**, *5*, 100059. [[CrossRef](#)]
10. Sillman, S. The relation between ozone, NO<sub>x</sub> and hydrocarbons in urban and polluted 744 rural environments. *Atmos. Environ.* **1999**, *33*, 1821–1845. [[CrossRef](#)]
11. Souri, A.H.; Nowlan, C.R.; Wolfe, G.M.; Lamsal, L.N.; Miller, C.E.C.; Abad, G.G.; Janz, S.J.; Fried, A.; Blake, D.R.; Weinheimer, A.J.; et al. Revisiting the effectiveness of HCHO/NO<sub>2</sub> ratios for inferring ozone sensitivity to its precursors using high resolution airborne remote sensing observations in a high ozone episode during the KORUS-AQ campaign. *Atmos. Environ.* **2020**, *224*, 117341. [[CrossRef](#)]
12. Richter, A.; Burrows, J.P.; Nusz, H.; Granier, C.; Niemeier, U. Increase in tropospheric nitrogen dioxide over China observed from space. *Nat. Cell Biol.* **2005**, *437*, 129–132. [[CrossRef](#)] [[PubMed](#)]
13. Li, X.; Brauers, T.; Hofzumahaus, A.; Lu, K.; Li, Y.P.; Shao, M.; Wagner, T.; Wahner, A. MAX-DOAS measurements of NO<sub>2</sub>, HCHO and CHOCHO at a rural site in Southern China. *Atmos. Chem. Phys. Discuss.* **2013**, *13*, 2133–2151. [[CrossRef](#)]
14. Feng, J.; Yu, H.; Su, X.; Liu, S.; Li, Y.; Pan, Y.; Sun, J.-H. Chemical composition and source apportionment of PM<sub>2.5</sub> during Chinese Spring Festival at Xinxiang, a heavily polluted city in North China: Fireworks and health risks. *Atmos. Res.* **2016**, *182*, 176–188. [[CrossRef](#)]
15. Tang, M.; Ji, D.-S.; Gao, W.-K.; Yu, Z.-W.; Chen, K.; Cao, W. Characteristics of air quality in Tianjin during the Spring Festival period of 2015. *Atmos. Ocean Sci. Lett.* **2016**, *9*, 15–21. [[CrossRef](#)]
16. Wang, C.; Huang, X.-F.; Zhu, Q.; Cao, L.-M.; Zhang, B.; He, L.-Y. Differentiating local and regional sources of Chinese urban air pollution based on the effect of the Spring Festival. *Atmos. Chem. Phys.* **2017**, *17*, 9103–9114. [[CrossRef](#)]
17. Yao, L.; Wang, D.; Fu, Q.; Qiao, L.; Wang, H.; Li, L.; Sun, W.; Li, Q.; Wang, L.; Yang, X. The effects of firework regulation on air quality and public health during the Chinese Spring Festival from 2013 to 2017 in a Chinese megacity. *Environ. Int.* **2019**, *126*, 96–106. [[CrossRef](#)]
18. Chen, C.; Sun, Y.L.; Xu, W.Q.; Du, W.; Zhou, L.B.; Han, T.T.; Wang, Q.Q.; Fu, P.Q.; Wang, Z.F.; Gao, Z.Q. Characteristics and sources of submicron aerosols above the urban canopy (260 m) in Beijing, China, during the 2014 APEC summit. *Atmos. Chem. Phys.* **2015**, *15*, 12879–12895. [[CrossRef](#)]
19. Ding, J.; van der A, R.J.; Mijling, B.; Levelt, P.F.; Hao, N. NO<sub>x</sub> emission estimates during the 2014 Youth Olympic Games in Nanjing. *Atmos. Chem. Phys.* **2015**, *15*, 9399–9412. [[CrossRef](#)]
20. Okuda, T.; Matsuura, S.; Yamaguchi, D.; Umemura, T.; Hanada, E.; Orihara, H.; Tanaka, S.; He, K.; Ma, Y.; Cheng, Y.; et al. The impact of the pollution control measures for the 2008 Beijing Olympic Games on the chemical composition of aerosols. *Atmos. Environ.* **2011**, *45*, 2789–2794. [[CrossRef](#)]
21. Xu, H.M.; Tao, J.; Ho, S.S.H.; Ho, K.F.; Cao, J.J.; Li, N.; Chow, J.C.; Wang, G.H.; Han, Y.M.; Zhang, R.J. Characteristics of fine particulate non-polar organic compounds in Guangzhou during the 16th Asian Games: Effectiveness of air pollution controls. *Atmos. Environ.* **2013**, *76*, 94–101. [[CrossRef](#)]
22. Zhao, J.; Du, W.; Zhang, Y.; Wang, Q.; Chen, C.; Xu, W.; Han, T.; Wang, Y.; Fu, P.; Wang, Z. Insights into aerosol chemistry during the 2015 China Victory Day parade: Results from simultaneous measurements at ground level and 260m in Beijing. *Atmos. Chem. Phys.* **2017**, *17*, 3215. [[CrossRef](#)]
23. Sharma, S.; Zhang, M.; Anshika; Gao, J.; Zhang, H.; Kota, S.H. Effect of restricted emissions during COVID-19 on air quality in India. *Sci. Total Environ.* **2020**, *728*, 138878. [[CrossRef](#)] [[PubMed](#)]
24. Dantas, G.; Siciliano, B.; França, B.B.; da Silva, C.M.; Arbilla, G. The impact of COVID-19 partial lockdown on the air quality of the city of Rio de Janeiro, Brazil. *Sci. Total Environ.* **2020**, *729*, 139085. [[CrossRef](#)] [[PubMed](#)]
25. Fan, C.; Li, Y.; Guang, J.; Li, Z.; Elnashar, A.; Allam, M.; de Leeuw, G. The Impact of the Control Measures during the COVID-19 Outbreak on Air Pollution in China. *Remote Sens.* **2020**, *12*, 1613. [[CrossRef](#)]
26. Muhammad, S.; Long, X.; Salman, M. COVID-19 pandemic and environmental pollution: A blessing in disguise? *Sci. Total Environ.* **2020**, *728*, 138820. [[CrossRef](#)]
27. Tobías, A.; Carnerero, C.; Reche, C.; Massagué, J.; Via, M.; Minguillón, M.C.; Alastuey, A.; Querol, X. Changes in air quality during the lockdown in Barcelona (Spain) one month into the SARS-CoV-2 epidemic. *Sci. Total Environ.* **2020**, *726*, 138540. [[CrossRef](#)]
28. Collivignarelli, M.C.; Abbà, A.; Bertanza, G.; Pedrazzani, R.; Ricciardi, P.; Carnevale Miino, M. Lockdown for CoViD-2019 in Milan: What are the effects on air quality? *Sci. Total Environ.* **2020**, *732*, 139280. [[CrossRef](#)]
29. Platt, U.; Stutz, J. *Differential Optical Absorption Spectroscopy—Principles and Applications*; Springer: Berlin/Heidelberg, Germany, 2008.
30. Ma, J.Z.; Beirle, S.; Jin, J.L.; Shaiganfar, R.; Yan, P.; Wagner, T. Tropospheric NO<sub>2</sub> vertical column densities over Beijing: Results of the first three years of ground-based MAXDOAS measurements (2008–2011) and satellite validation. *Atmos. Chem. Phys.* **2013**, *13*, 1547–1567. [[CrossRef](#)]

31. Chan, K.L.; Hartl, A.; Lam, Y.F.; Xie, P.H.; Liu, W.Q.; Cheung, H.M.; Lampel, J.; Pöhler, D.; Li, A.; Xu, J.; et al. Observations of tropospheric NO<sub>2</sub> using ground based MAX-DOAS and OMI measurements during the Shanghai World Expo 2010. *Atmos. Environ.* **2015**, *119*, 45–58. [[CrossRef](#)]
32. Chan, K.L.; Wiegner, M.; Wenig, M.; Pöhler, D. Observations of tropospheric aerosols and NO<sub>2</sub> in Hong Kong over 5 years using ground based MAX-DOAS. *Sci. Total Environ.* **2018**, *619–620*, 1545–1556. [[CrossRef](#)]
33. Clémer, K.; Van Roozendaal, M.; Fayt, C.; Hendrick, F.; Hermans, C.; Pinardi, G.; Spurr, R.; Wang, P.; De Mazière, M. Multiple wavelength retrieval of tropospheric aerosol optical properties from MAXDOAS measurements in Beijing. *Atmos. Meas. Tech.* **2010**, *3*, 863–878. [[CrossRef](#)]
34. Cheng, Y.; Wang, S.; Zhu, J.; Guo, Y.; Zhang, R.; Liu, Y.; Zhang, Y.; Yu, Q.; Ma, W.; Zhou, B. Surveillance of SO<sub>2</sub> and NO<sub>2</sub> from ship emissions by MAX-DOAS measurements and the implications regarding fuel sulfur content compliance. *Atmos. Chem. Phys.* **2019**, *19*, 13611–13626. [[CrossRef](#)]
35. Zhang, J.; Wang, S.; Guo, Y.; Zhang, R.; Qin, X.; Huang, K.; Wang, D.; Fu, Q.; Wang, J.; Zhou, B. Aerosol vertical profile retrieved from ground-based MAX-DOAS observation and characteristic distribution during wintertime in Shanghai, China. *Atmos. Environ.* **2018**, *192*, 193–205. [[CrossRef](#)]
36. Danckaert, T.; Fayt, C.; Van Roozendaal, M.; De Smedt, I.; Letocart, V.; Merlaud, A.; Pinardi, G. *QDOAS Software User Manual*; Belgian Institute for Space Aeronomy: Brussels, Belgium, 2013.
37. Chance, K.; Kurucz, R.L. An improved high-resolution solar reference spectrum for earth's atmosphere measurements in the ultraviolet, visible, and near infrared. *J. Quant. Spectrosc. Radiat. Transf.* **2010**, *111*, 1289–1295. [[CrossRef](#)]
38. Meller, R.; Moortgat, G.K. Temperature dependence of the absorption cross sections of formaldehyde between 223 and 323 K in the wavelength range 225–375 nm. *J. Geophys. Res. Space Phys.* **2000**, *105*, 7089–7101. [[CrossRef](#)]
39. Vandaele, A.C.; Hermans, C.; Simon, P.C.; Carleer, M.; Colin, R.; Fally, S.; Merienne, M.-F.; Jenouvrier, A.; Coquart, B. Measurements of the NO<sub>2</sub> absorption cross-section from 42000 cm<sup>-1</sup> to 10000 cm<sup>-1</sup> (238–1000 nm) at 220 K and 294 K. *J. Quant. Spectrosc. Radiat. Transf.* **1998**, *59*, 171–184. [[CrossRef](#)]
40. Fleischmann, O.C.; Hartmann, M.; Burrows, J.P.; Orphal, J. New ultraviolet absorption cross-sections of BrO at atmospheric temperatures measured by time-windowing Fourier transform spectroscopy. *J. Photochem. Photobiol. A Chem.* **2004**, *168*, 117–132. [[CrossRef](#)]
41. Serdyuchenko, A.; Gorshchev, V.; Weber, M.; Chehade, W.; Burrows, J.P. High spectral resolution ozone absorption cross-sections—Part 2: Temperature dependence. *Atmos. Meas. Tech.* **2014**, *7*, 625–636. [[CrossRef](#)]
42. Thalman, R.; Volkamer, R. Temperature dependent absorption cross-sections of O<sub>2</sub>–O<sub>2</sub> collision pairs between 340 and 630 nm and at atmospherically relevant pressure. *Phys. Chem. Chem. Phys.* **2013**, *15*, 15371–15381. [[CrossRef](#)]
43. Wagner, T.; Ibrahim, O.; Shaiganfar, R.; Platt, U. Mobile MAX-DOAS observations of tropospheric trace gases. *Atmos. Meas. Tech.* **2010**, *3*, 129–140. [[CrossRef](#)]
44. Solomon, S.; Schmeltekopf, A.L.; Sanders, R.W. On the interpretation of zenith sky absorption measurements. *J. Geophys. Res. Space Phys.* **1987**, *92*, 8311–8319. [[CrossRef](#)]
45. Celarier, E.A.; Brinksma, E.J.; Gleason, J.F.; Veefkind, J.P.; Cede, A.; Herman, J.R.; Ionov, D.; Goutail, F.; Pommereau, J.; Lambert, J. Validation of Ozone Monitoring Instrument nitrogen dioxide columns. *J. Geophys. Res. Space Phys.* **2008**, *113*. [[CrossRef](#)]
46. Stein, A.F.; Draxler, R.R.; Rolph, G.D.; Stunder, B.J.B.; Cohen, M.D.; Ngan, F. NOAA's HYSPLIT Atmospheric Transport and Dispersion Modeling System. *Bull. Am. Meteorol. Soc.* **2015**, *96*, 2059–2077. [[CrossRef](#)]
47. Zhan, D.; Kwan, M.; Zhang, W.; Yu, X.; Meng, B.; Liu, Q. The driving factors of air quality index in China. *J. Clean. Prod.* **2018**, *197*, 1342–1351. [[CrossRef](#)]
48. Cleveland, W.S.; Graedel, T.E.; Kleiner, B.; Warner, J.L. Sunday and workday variations in photochemical air pollutants in New Jersey and New York. *Science* **1974**, *186*, 1037–1038. [[CrossRef](#)]
49. Stockwell, W.R.; Forkel, R. Ozone and volatile organic compounds: Isoprene, terpenes, aldehydes, and organic acids. In *Trace Gas Exchange in Forest Ecosystems*; Springer: Berlin/Heidelberg, Germany, 2002; pp. 257–276.
50. Sillman, S. The use of NO<sub>y</sub>, H<sub>2</sub>O<sub>2</sub>, and HNO<sub>3</sub> as indicators for ozone-NO<sub>x</sub>-hydrocarbon sensitivity in urban locations. *J. Geophys. Res. Atmos.* **1995**, *100*, 14175–14188. [[CrossRef](#)]
51. Duncan, B.N.; Yoshida, Y.; Sillman, S.; Retscher, C.; Pickering, K.E.; Martin, R.V.; Celarier, E.A. The Sensitivity of US Surface Ozone Formation to NO<sub>x</sub> and VOCs as Viewed from Space. In Proceedings of the 8th Annual CMAS Conference, Chapel Hill, NC, USA, 19–21 October 2009.
52. Javed, Z.; Liu, C.; Khokhar, M.F.; Xing, C.; Tan, W.; Subhani, M.A.; Rehman, A. and Tanvir, A. Investigating the impact of Glyoxal retrieval from MAX-DOAS observations during haze and non-haze conditions in Beijing. *J. Environ. Sci.* **2019**, *80*, 296–305. [[CrossRef](#)]
53. Li, L.; Li, Q.; Huang, L.; Wang, Q.; Zhu, A.; Xu, J.; Liu, Z.; Li, H.; Shi, L.; Li, R.; et al. Air quality changes during the COVID-19 lockdown over the Yangtze River Delta Region: An insight into the impact of human activity pattern changes on air pollution variation. *Sci. Total Environ.* **2020**, *732*, 139282. [[CrossRef](#)]
54. Ali, S.M.; Malik, F.; Anjum, M.S.; Siddiqui, G.F.; Anwer, M.N.; Lam, S.S.; Nizami, A.S.; Khokhar, M.F. Exploring the linkage between PM<sub>2.5</sub> levels and COVID-19 spread and its implications for socio-economic circles. *Environ. Res.* **2020**, *193*, 110421. [[CrossRef](#)]

- 
55. Kerimray, A.; Baimatova, N.; Ibragimova, O.P.; Bukenov, B.; Kenessov, B.; Plotitsyn, P.; Karaca, F. Assessing air quality changes in large cities during COVID-19 lockdowns: The impacts of traffic-free urban conditions in Almaty, Kazakhstan. *Sci. Total Environ.* **2020**, *730*, 139179. [[CrossRef](#)]
  56. Mahato, S.; Pal, S.; Ghosh, K.G. Effect of lockdown amid COVID-19 pandemic on air quality of the megacity Delhi, India. *Sci. Total. Environ.* **2020**, *730*, 139086. [[CrossRef](#)] [[PubMed](#)]
  57. Javed, Z.; Wang, Y.; Xie, M.; Tanvir, A.; Rehman, A.; Ji, X.; Xing, C.; Shakoor, A.; Liu, C. Investigating the Impacts of the COVID-19 Lockdown on Trace Gases Using Ground-Based MAX-DOAS Observations in Nanjing, China. *Remote Sens.* **2020**, *12*, 3939. [[CrossRef](#)]